A NUMERICAL INVESTIGATION OF PLANE STRAIN STABLE CRACK GROWTH UNDER SMALL SCALE YIELDING CONDITIONS†

E. Paul Sorensen*

September 1977

*Research Assistant, Division of Engineering, Brown University, Providence, RI 02912

†This paper will be presented at the ASTM Symposium on Elastic-Plastic Fracture, Atlanta, November 1977.

DISCLAIMER

ABSTRACT

Plane strain crack advance under small scale yielding conditions in elastic-perfectly plastic and power law hardening materials is investigated numerically via the finite element method. Results indicate that the stress distribution ahead of a growing crack is essentially the same as that ahead of a stationary crack, and the numerically evaluated steady state crack tip profiles reflect a vertical tangent at the extending crack tip which corresponds to the theoretically predicted outline. It is found that the increment $d\delta_t$ in crack tip opening, when loads are increased at fixed crack length, seems to be uniquely related to dJ/σ_o irrespective of the amount of previous crack growth, and for increments $d\ell$ of crack advance at constant external load, this quantity appears related to $\frac{J}{\sigma_o r} d\ell$ when evaluated at distance r from the tip. A discussion of proposed fracture parameters for continued crack growth (as opposed to growth initiation) is included.

KEY WORDS: stable crack growth, small scale yielding, non-hardening and power law hardening materials, fracture criteria for continued crack advance.

INTRODUCTION

The stress and strain fields associated with stationary cracks have been widely explored, e.g., Rice [1]. Elastic, elastic-plastic, and viscoelastic constitutive behavior under small strain conditions have been examined among other idealizations, and some solutions exist which account for the finite geometry changes present in the immediate vicinity of a blunted crack tip [2], [3]. Plane stress, plane strain and axisymmetric configurations have been analyzed as well as three dimensional bodies. All three modes of loading (viz. the opening or tensile mode, in-plane shear, and out-of-plane shear) have been considered; some mixed mode loading solutions also exist [4]. These extensive investigations have revealed various correlations between the "state" at the crack tip and macroscopic parameters such as the J integral and the crack opening displacement.

In contrast to the extensive literature pertinent to stationary cracks, a paucity of solutions for the growing crack situation is evident. One obvious reason for this is the added mathematical complexity inherent in a continuum formulation of the growing crack. Also, design procedures which equate the failure of a component with the initial crack extension event may be overly conservative and a complete theory of fracture must include a region of slow, stable crack extension between the inception of crack propagation and final, fast or catastrophic failure.

An analytic investigation of the extending crack problem under Mode III conditions is presented by McClintock [5] with elaborations and amplifications provided by McClintock and Irwin [6] and Rice [7], [8].

These solutions treat the crack advance as quasistatic and consider elastic-perfectly plastic material behavior. One conclusion of these studies is that the strain field ahead of an extending crack is dominated by a logarithmic singularity which is weaker than the $1/r$ singularity experienced at the tip of a stationary crack (where r is distance measured from the crack tip). The weaker strain singularity is due to the crack extending into material that has deformed plastically so that complete refocusing of the strain field at the tip of the extended crack is prevented. This reduced crack tip strain concentration is a primary cause of stable crack growth in elastic-plastic materials. The Mode III analyses coupled with an arbitrarily chosen fracture criterion suggest that for ductile materials the initiation of crack propagation and final instability are separated by a region of stable crack growth in which it is possible for a component to support additional load. This observation provides additional motivation for the study of stable crack growth: the added load bearing capacity of components designed with stable crack growth considerations.

Detailed solutions to crack extension problems in Mode I are more difficult to obtain. Rice [7] discusses the form of the solution to such a plane strain problem in an elastic-perfectly plastic material under steady state conditions, and in [8] Rice presents various aspects of the incremental solution to this crack growth problem. In a small scale yielding, incremental formulation the total strain increment is derived from the incremental displacements, and the plastic strain increment is calculated as the difference between the total increment of strain and the elastic increment of strain, related to the stress field through Hooke's law.

This stress field is given by the Prandtl slip line construction and singular strain rates result in the "centered fan" portions above and below the crack tip; the stress distribution moves relative to the material. This incompatible elastic strain increment induces plastic strain during an increment of crack advance and it is not derivable from a displacement field. The additional straining promotes fast crack growth due to the increased strain concentration accumulated at the crack tip. Integration of the plastic strain increments results in a term which is logarithmically singular in r and which obtains contributions only from the centered fan regions above and below the crack tip. On average then, the crack advances between these centered fan sectors. Another consequence of the elastic incompatibility is that contrary to the rigid plastic case in which the crack advances with a finite crack tip opening angle, the elastic-plastic incremental formulation results in a crack face profile exhibiting a vertical tangent at the crack tip and a corresponding ill-defined crack tip opening angle. Both the rigid-plastic case and the elastic-perfectly plastic case predict a zero crack opening displacement at the tip of an extending crack. In this respect, the Mode III, asymptotic analysis presented by Chitaley and McClintock [9] is incorrect in its prediction of a non-zero crack opening displacement at the tip of a steadily extending crack, and the difficulty seems to arise from their approximate numerical evaluation of an integral which should have given zero for a result [8].

An important omission of the above analyses is the finite geometry changes and associated large strain fields surrounding a blunted crack tip. Also, no account is taken of the Bauschinger effect or possible vertex

developments on the yield surface during the non-radial loading experienced by material points during crack growth. These effects could lead to additional strain accumulations at the crack tip and as such reduce any stable crack growth regimes.

Experimental observations of stable crack growth have been reported by several authors. Broek [10] reports stable crack growth under plane stress and plane strain conditions and emphasizes that crack growth initiation, stable crack extension, and final fast fracture must be considered as contiguous phases of crack propagation. Green et al. [11] discuss effects of a dual fracture mode: fracture governed by shear lips at the sides of a specimen and by plane strain considerations in the middle region of thicker specimens. This "thumbnail" characterization of crack advance is further investigated with regard to thickness effects by Green and Knott [12]. The picture that emerges from these investigations is that as the thickness of a specimen increases the proportion of flat crack front increases with the shear lip extent virtually unchanged. Green and Knott [12] observe a constant increase in the nominal crack opening displacement per increment of crack growth and conclude that the crack face profile associated with an extending crack tip in a ductile metal is constant. They also present a model based on growth between equally-spaced inclusions which predicts a constant crack tip opening angle. J integral experimentation due to Clarke et al. [13] and Griffis and Yoder [14] indicates a constant change of J with change of crack length following the blunting of an initially sharp crack. The implication is that the advancing crack tip experiences constant surrounding fields. These results are analogous if we imagine that

J and δ remain linearly related as they are in the stationary crack case.

A critical observation made by Green and coworkers is that crack advance may occur at a constant load level which is below load levels usually associated with the instability of various components. The present analyses, however, may not explore this point due to the rate independent plasticity model employed.

Finite element solutions to extending cracks include the work of de Koning [15] who studies the growth of cracks under plane stress conditions and compares his numerical results with experimental observations on geometrically similar specimens. Andersson [16] studies steady state results for cracks in anti-plane strain and plane stress loading modes. Sorensen [17] presents results for various Mode III analyses of moving cracks. A key objective of the numerical solutions, aside from the illumination of the stress and strain distributions accompanying growing cracks, is the investigation of possible macroscopic parameters which may be correlated with the "state" at the growing crack tip. Although the meaning of the J integral is unclear in the growing crack case, J is known to rise monotonically with crack advance, e.g., [13], and its use as a fracture predictor in the extending crack case is a possibility. Other proposed parameters are the crack tip opening angle, [18], which is taken to be a material property and the Griffith-like separation energy rate associated with a finite crack advance step, [19].

NUMERICAL CONSIDERATIONS

Finite Element Equations

A form of the virtual work equation, valid for incremental small strain theory in which all integrals are carried out over the reference volume and surface, is used in the derivation of the governing finite element equations:

$$\int_V \dot{\sigma}_{ij}\, \delta\dot{u}_{j,i}\, dV = \int_S \dot{T}_i\, \delta\dot{u}_i\, dS \quad ,$$

where u_i is the displacement vector, T_i is the traction vector, σ_{ij} is the Cauchy stress tensor, and superimposed dots denote rates. Let [N] denote the shape functions used to represent variations of displacement within an element as interpolated from nodal displacement values, {u} , so that [N]{u} represents the displacement field. The incremental strain-displacement relation is $\{\dot{\varepsilon}\} = [B]\{\dot{u}\}$, where [B] is composed of the appropriate derivatives of [N]. The constitutive matrix is denoted by [C] such that the incremental stress is related to the incremental strain by $\{\dot{\sigma}\} = [C]\{\dot{\varepsilon}\}$. Substituting the above matrix relations into the governing variational equation and recognizing that arbitrary variations may not influence the resulting equilibrium equations, one obtains the well known tangent stiffness equations:

$$\left(\int_V [B]^T [C]\, [B]\, dV\right) \{\dot{u}\} = \int_S [N]^T \{\dot{T}\}\, dS$$

where integrals are carried out over all elements and over all externally loaded surfaces. In conventional finite element notation this equation is written $[K]\{\dot{u}\} = \{\dot{P}\}$ with [K] termed the master stiffness matrix and {P} the forcing function or right hand side.

Constitutive Relations

The material constitutive behavior is modelled as isotropic, elastic-perfectly plastic and elastic power-law hardening together with the Mises yield condition and the associated Prandtl-Reuss flow law [20]. The power law hardening relation is that used by Tracey [21], namely $\bar{\sigma}/\sigma_o = (\bar{\sigma}/\sigma_o + 3G\bar{e}^p/\sigma_o)^N$, where N is the hardening exponent, G is the shear modulus, σ_o is the yield stress in tension, $\bar{\sigma} = \sqrt{\frac{3}{2} s_{ij}s_{ij}}$, s_{ij} is the deviatoric Cauchy stress tensor, $\bar{e}^p = \sqrt{\frac{2}{3} e^p_{ij} e^p_{ij}}$ and e^p_{ij} is the plastic portion of the deviatoric strain tensor. This power law hardening expression is obtained from the relation $\bar{\tau}/\tau_o = (\bar{\gamma}/\gamma_o)^N$ for pure shear used by Rice and Rosengren [22] through the conversions $\bar{\tau} = \bar{\sigma}/\sqrt{3}$, $\bar{\gamma}^p = \sqrt{3}\,\bar{e}^p$ and $\bar{\gamma} = \bar{\gamma}^e + \bar{\gamma}^p$. No account is taken of the Bauschinger effect or possible vertex development of the yield surface during the non-radial loading experienced by material points during crack growth. These omissions must be kept in mind during the interpretation of the present results. The non-linear problem is linearized by specifying small load increments and iterating within each increment for convergence to the best representative plastic constitutive matrices. The constitutive matrix [C] at any point in the loading history may be written as

$$[C] = m[C^{el}] + (1-m)\,[C^{el-pl}]$$

with $0 \le m \le 1$. This partial stiffness approach is due to Marcal and King [23]. $[C^{el-pl}]$ is determined from the normal to the yield surface and m depends on the amount of elastic response an element undergoes during a load increment (i.e., $m = 1$ for totally elastic response and $m = 0$ for totally plastic response). The normal used in these expressions is chosen

in the manner of Rice and Tracey [24] such that resulting stress states precisely satisfy the yield criterion in the elastic-perfectly plastic case and approximately satisfy the yield criterion in the power law hardening case [21]. Typically 2 to 3 iterations are required per loading increment for convergence to an appropriate constitutive representation. Reassembly and redecomposition of the master stiffness matrix is accomplished in a cost minimizing manner, using the efficient procedure discussed by Yang [25] and Sorensen [26] and various in-and-out of core procedures we required [27].

Crack Growth Simulation

A nodal release technique is implemented to simulate crack advancement through the finite element mesh. This technique is used by Andersson [18] and by Kfouri and Miller [19]. As applied here, the technique proceeds as follows: upon satisfaction of a chosen fracture criterion, the crack is deemed ready to propagate and the boundary condition at the crack tip passes from displacement controlled to traction controlled. The reaction force corresponding to the zero displacement condition at the crack tip node is calculated and relaxed to zero in five equal increments. Following this procedure, the crack tip has advanced by one element length. The present analysis holds external loads constant during the nodal relaxation procedure. It is anticipated that due to the history dependence of the strain distribution the process of nodal force relaxation under increasing external load might result in a somewhat different strain state ahead of the crack tip from that obtained under constant external load. The present results are interpreted as representative of crack advance under constant load or perhaps under slight increases of external load.

Element Modelling

The element used in the present analyses is the constant strain triangle, Turner et al. [28]. Quadrilaterals are formed from four of these elements in the manner of Nagtegaal et al. [29] to accommodate the possibility of nearly incompressible straining, and the degrees of freedom associated with the internal node are eliminated from the stiffness equations, [30]. This configuration in no way accounts for the mathematical singularities encountered at the crack tip but useful results are obtained by sufficient mesh refinement (see discussion of results). Due to the nodal release technique employed in the analyses, no use of special crack tip singular elements, e.g., Tracey [31] and Wilson [32], is made since the crack advance would require a procedure for refocusing the mesh at the tip of the extended crack. In this context an Eulerian finite element formulation holds much promise, for then a mesh remains focused at the crack tip and singularity elements may be employed; however, such a formulation presents other difficulties such as the convective terms which require spatial derivatives of field quantities and an economically feasible formulation has not yet been found.

Numerical Procedure

Following an elastic increment in which the highest stressed element is scaled to cause incipient yielding, various increments of load equal to 10 or 20% of that in the initial solution are carried out. The nodal release procedure is implemented upon achievement of the static similarity solution of Tracey [21] and further loading is applied at the new crack length. Various steps of crack advance and external loading at constant crack length are performed. Displacement boundary conditions corresponding to the elastic

singular strain dominant at the crack tip are specified on a radius which is 224 times the smallest element size and 20 times the maximum extent which the plastic zone acquires in the course of the computation. These ratios insure an appropriate boundary layer formulation of the small scale yielding situation [7]. The next term beyond the inverse square root singularity in the surrounding elastic field, namely a tension T parallel to the crack, is taken as zero. Figure 1 presents the load histories relevant to the analyses presented here; in this figure, K_o is the stress intensity factor at the first load increment, σ_o is the yield stress in tension, and $\ell-\ell_o$ is the difference between the current and initial crack lengths. These "staircase" load histories represent hypothetical cases which might be found in service.

Mesh Configuration and Material Properties

The finite element grid used in these analyses is indicated in figure 2 with details of the refined mesh surrounding the crack tip presented in figure 3. A total of 1660 elements is used together with 865 nodes and 1730 degrees of freedom. Use of static condensation reduces the number of active degrees of freedom to 946. The radius of the outer ring in figure 3 divided by the smallest element length is 28. The radii of the rings in figure 2 divided by the inner element length are 28., 34., 42., 52., 64., 80., 104., 136., 176. and 224. The radial lines are spaced at 10 degree intervals. Material properties are $\nu = .3$ and $E/\sigma_o = 1000$ where E is Young's modulus and σ_o the tensile yield strength. The analysis corresponding to the ideal plasticity case was carried out on the IBM 360/67 available at Brown University Computing Laboratory. The two hardening analyses were performed using the IBM 370/168 available at the Massachusetts Institute of Technology.

RESULTS AND DISCUSSION

Crack Face Profiles

Figure 4 presents crack face profiles following the load incrementation procedure for the stationary crack and following the final crack advance step for the cases $N = 0.0$, 0.1 and 0.2. The profiles following the final crack advance step are considered representative of steady state conditions in the vicinity of the crack tip but not overall as away from the crack tip the crack faces experience continuing deformation. Direct comparisons of the stationary crack profiles with those of Tracey [21] indicate maximum deviations of 6%, 5% and 3% for $N = 0.0$, 0.1 and 0.2 respectively. Since the present analyses do not employ special singularity elements like those of Tracey [31] and do not include finite geometry changes, the crack tip opening displacements, δ, are estimated by extrapolation. For the non-hardening case, a value of 0.66 is obtained for δ nondimensionalized by J/σ_o, where J is taken equal to $(1-\nu^2)K_I^2/E$ corresponding to the small scale yielding situation. Tracey predicts a value of 0.54 for this ratio, but Parks [33] suggests that this number should be 0.65 due to the artificial path dependence of J that seems (through comparison with a corresponding "deformation theory" solution based on Tracey's mesh, leading to similar path-dependence) to be directly traceable to Tracey's non-hardening singularity element. For non-hardening blunting solutions, McMeeking [3] reports values for the non-dimensionalized crack opening displacement between 0.55 and 0.67 depending on the point of measurement. The larger of these two numbers is representative of larger values of σ_o/E, on the order of $1/100$. For σ_o/E equal to $1/300$ and $N = 0.1$, McMeeking reports values of the non-dimensionalized crack opening displacement between 0.41 and 0.44, and for $N = 0.2$ values between 0.27 and 0.30

are reported, although higher values result when measured at the elastic plastic boundary. The present hardening analyses predict a value of 0.54 for the non-dimensionalized crack opening displacement when $N = 0.1$ and 0.44 when the hardening exponent equals 0.2. The good agreement of the extrapolated values of δ with the work of McMeeking and others lends confidence to the results of the present analyses as regards the prediction of the crack face profiles.

Figure 5 presents crack face profiles at key points in the evolution of the prescribed load history for the non-hardening case. This analysis, which models crack growth at constant load between equidistant nodal points in rate independent materials, results in a crack face profile which as the crack advances becomes less angular with distance from the crack tip (where the "angle" is measured clockwise from a horizontal line behind the crack tip). This is also true for the hardening cases as indicated by the final crack profiles shown on figure 4. Rice [7], [8],for quasistatic crack advance in a non-hardening material, derives a displacement distribution proportional to $r \ln r$ (where r is the radial distance measured from the crack tip) which implies a vertical tangent at $r = 0$. Nodal displacements from the present analyses permit curve fairing which exhibit the vertical tangent required by the analytic solution. This infinite slope is a local phenomenon and may not overly influence the effective definition of a crack tip opening angle, defined here as the total angle between the separating crack faces behind the extending crack tip. However, this remains an open issue in need of further study. Due to the linear interpolation functions used in the present analysis, this angle is evaluated at the node immediately behind the crack tip and resulting values are presented in Table I. The trend towards a steady state value is

anticipated from the prescribed loading, and the numbers in Table I indicate the material dependent nature of the crack tip opening angle. As the final displacement distributions on figure 4 suggest, the angles would be less if based on elements further back from the crack tip, and the parameter seems to be meaningless according to theoretical considerations in the limit of r approaching zero. To further clarify the role of the crack tip opening angle and its relation to continuing fracture, a finite strain analysis in the spirit of McMeeking [3] is desirable for the region in the vicinity of the crack tip.

Prior to any crack advance, the crack opening displacement is related to the external loading according to $\delta = \alpha J/\sigma_o$, where α is dependent on material properties and hardening exponent. As previously remarked, values of α for the stationary portion of the present analyses are 0.66, 0.54 and 0.44 which agree well with published values. Following crack advance, the load histories prescribe increments of external load at constant crack length, and a relation between incremental crack opening displacement and increments in external loads is

$$d\delta = \alpha \frac{dJ}{\sigma_o} \quad . \tag{1}$$

Values of α in this relation are presented in Table II; increments in crack opening displacement are measured at the node immediately behind the current crack tip and the original crack tip position. The numbers in Table II indicate that the nominal crack tip opening displacement continues to be effectively characterized by increments in J for external loading at fixed crack length following crack advance steps. For each of these analyses, α seems to be constant, namely 0.66, 0.54 and 0.44 for $N = 0.0$, 0.1 and 0.2 respectively.

The present analyses prescribe crack advance at constant external load, and here the resulting incremental crack surface displacements are related to the crack advance step. Rice [8] obtains a relation between incremental displacements resulting from an increment of crack advance, $d\ell$, and the increment of crack advance. This relation may be written as

$$du_i = \frac{\sigma_o}{E}\left[A_i(\theta) + B_i(\theta)\, \ell n \frac{R}{r}\right] d\ell \quad ,$$

where $A_i(\theta)$ and $B_i(\theta)$ are dimensionless functions and R is a characteristic length of the plastic zone. Noting that for small scale yielding R scales with EJ/σ_o^2, and specializing the above expression to the crack surface $(\theta = \pi)$, the following is obtained

$$d\delta = \frac{\sigma_o}{E}\, \beta\, \ell n \left[\lambda \frac{EJ}{\sigma_o^2 r}\right] d\ell \quad . \tag{2}$$

Here, the proportionality constants have been lumped into β and λ, and $d\delta$ is the crack opening displacement increment. Equation (2) may be integrated to obtain an expression for the additional crack opening displacement resulting at a fixed point X as the crack advances under constant J from ℓ_1 to ℓ_2, two crack lengths such that $\ell_2 > \ell_1 \geq X$. The integration results in

$$\delta(\ell_2,X) - \delta(\ell_1,X) = \beta \frac{\sigma_o}{E}\left[(\ell_2-X)\ell n \frac{\lambda e EJ}{\sigma_o^2(\ell_2-X)} - (\ell_1-X)\ell n \frac{\lambda e EJ}{\sigma_o^2(\ell_1-X)}\right] . \tag{3}$$

For the node immediately behind the advancing crack tip, $\ell_1 = X$ and the second term on both the left side and right side of (3) is zero. Figure 6 presents a plot of crack surface displacement values for the node immediately behind the crack tip taken from the present hardening and non-hardening analyses. The plot indicates a unique pair (β,λ) which satisfies

equation (3), namely $\beta = 9.5$ and $\lambda = .04$. These values of β and λ do not correctly predict the incremental crack opening displacement due to crack advance at the other nodes behind the advancing tip, indicating that (2) may apply only within a certain distance from the crack tip. This latter point is currently under further investigation. However, the good correlation provided by (2) for incremental crack opening near the advancing crack tip due to an increment in crack advance at constant external load indicates the possibility of using (2) in conjunction with (1) to provide a relationship for the characterization of incremental crack opening displacements with increments of external loads as well. That is,

$$d\delta = \alpha \frac{dJ}{\sigma_o} + \beta \frac{\sigma_o}{E} \ell n \frac{\lambda E J}{\sigma_o^2 r} d\ell \quad . \tag{4}$$

This equation appears useful in the study of continuing fracture and its use in developing a fracture criterion based on near-tip crack opening is presently under examination.

Stress Distributions Ahead of the Crack Tip

The stress fields associated with hardening and non-hardening plane strain, stationary cracks under small scale yielding conditions are provided by Tracey [21]. Figure 7 presents curves for the opening stress ahead of a stationary crack together with corresponding centroidal stress values of elements directly ahead of the crack tip taken from the present analyses. The distance from the crack tip to the centroid is used for the position on the abcissa of the plot. Maximum deviations of the present results from Tracey's curves are 5%, 5% and 7% for $N = 0.0$, 0.1 and 0.2 respectively. The good agreement of these values is a consequence of the fine mesh employed in the solution.

As the stress gradients near the crack tip become steeper with increasing hardening exponent, the deviations of the present results from those of Tracey are expected to increase since these analyses make no use of singular elements but rely on fine mesh gradation to capture the appropriate stress distributions. This formulation provides little information on the angular stress distribution as r approaches zero and does not precisely obtain the factor of 2.97 in σ_{22} stress elevation over σ_o as the Prandtl solution demands in the non-hardening case.

Figure 7 also indicates points corresponding to the apparently steady state stress distribution predicted in the present analyses. Following the final crack advance step, there are minor elevations of σ_{22} ahead of the tip with maximum deviations from Tracey's results for a stationary crack of 4%, 3% and 7% for $N = 0.0$, 0.1 and 0.2 . Similar plots of the σ_{22} stress distribution ahead of the crack tip following intermediate crack advance steps reveal points between the static and steady state points presented in figure 7. The conclusion is that under small scale yielding conditions for both hardening and non-hardening materials, the σ_{22} stress distribution ahead of a growing crack is effectively the same as the corresponding stress distribution for a stationary crack.

Material Stress Histories

Three material point stress histories are now described. The points under scrutiny are the element immediately behind the initial crack tip, an element ahead of the initial crack tip and on the prospective fracture plane and an element ahead of the initial crack tip but removed from the fracture plane. These material points are designated element A, B and C respectively and are indicated on figure 3. The stresses described are

centroidal stresses associated with the constant strain triangles used in the analyses.

Element A:

Following the final static load incrementation step, values of σ_{11}/σ_o are 1.14, 1.29 and 1.51, values of σ_{22}/σ_o are 1.27, 1.44 and 1.69 and values of σ_{12}/σ_o are -0.57, -0.69 and -0.86 for N = 0.0, 0.1 and 0.2 respectively. Upon subsequent crack advance and load incrementation steps, both σ_{12} and σ_{22} become small in contrast with σ_{11} which dominates the later stress history. After the last crack advance step, non-dimensionalized values of σ_{11} are 1.07, 1.13 and 1.06 for the three analyses. The final value of σ_{11} seems to represent a residual tensile stress in a plastic wake region. For the non-hardening case there is some continuing plastic flow in this wake, but not in the hardening cases. This is due to the isotropic model of strain hardening used in these analyses and underlines the sensitivity of the results to the constitutive model used. The Prandtl stress distribution suggests that $\sigma_{11} = 1.15\ \sigma_o$ on the crack surfaces immediately behind the crack tip, and the final value of σ_{11} in the non-hardening case is 7% below this number.

Element B:

This material point lies ahead of the initial crack tip but behind the final crack tip position in these analyses. This material experiences continued increases in σ_{11} and σ_{22} during the first two nodal release steps. Values of σ_{22}/σ_o following the second nodal release step are 2.74, 3.03 and 3.45 for N = 0.0, 0.1 and 0.2 respectively. Then, during the remaining nodal release steps σ_{22} drops to a small value and σ_{11} becomes the dominant stress at the point. It is not surprising that σ_{22} should drop

drastically, because the traction free boundary condition imposed on the open crack face requires that σ_{22} be zero there (assuming negligible deviation of the surface normal from the X_2 direction). Also, following the third nodal release step during which this element becomes part of the material behind the crack tip, values of σ_{12}/σ_o are -0.56, -0.67 and -0.80 for the three hardening exponents. For the non-hardening case, σ_{11} and σ_{22} are nearly equal and this is consistent with the notion that at this stage of its history the element is part of a centered fan above the crack tip requiring a hydrostatic stress state coupled with plastic shearing. Then as the crack advances further, this element passes from the centered fan region to a residually stressed wake region as discussed above.

Element C:

This element is further removed from the plane of fracture than element B above. Figure 8A presents a plot of its stress history versus crack advance step for the non-hardening case. This plot is also representative of the hardening results but with an appropriate shift of the vertical axis. Figure 8A also presents stresses as predicted from a Prandtl stress distribution travelling with the crack; the Prandtl slip line construction is indicated in figure 8B. The material point under discussion is imagined enveloped by region 1 in figure 8B following release 1, in the centered fan of region 2 following release 2 and 3 and in constant state region 3 following the final two steps of crack advance. For the stress values plotted in figure 8A, θ is taken as the angle between a horizontal line and a line joining the centroid of element C to the actual crack tip. The numerically calculated stress distribution reflects a pattern similar to that predicted by the Prandtl field. However, the fuzzy crack tip phenonenon is also evident. This terminology describes the consequences of a finite

element discretization which cannot exactly reproduce appropriate strain singularities at the crack tip so that elements surrounding the crack tip respond to an ill defined crack tip with a corresponding vagueness in the definition of θ and r. This effect is minimized as the mesh is refined.

These brief descriptions of material stress point histories reinforce the previously made point that the steady state σ_{22} stress distribution is effectively the same as that prior to any crack extension. Additional conclusions are: i) following crack advance steps, points positionally similar with respect to the crack tip experience similar stress histories of loading and unloading which suggests that a steady state prevails near the advancing crack tip. Positionally similar stress histories are a tacit assumption of the ideally plastic theoretical analysis of plastic strain singularities for growing cracks [7], [8] discussed earlier. ii) prior to any given nodal release step the elements surrounding the crack tip experience essentially the same stress field as those surrounding a stationary crack. This stress field, within the limitations of the present analyses, resembles the Prandtl slip line solution for the non-hardening situation. iii) the wake material is dominated by a residual, tensile σ_{11} stress which results in continued yielding in the non-hardening case, but not in the hardening cases due to the isotropic hardening model used.

Plastic Zone Shapes

The shapes of the active plastic zones, corresponding to the final static load increment and the final step of crack advance, nondimensionalized by the similarity quantity $(K_I/\sigma_o)^2$ are presented in figures 9A, 9B and 9C for the hardening exponents 0.0, 0.1 and 0.2 respectively. The plastic zone shapes corresponding to the static crack solutions are in good agreement with

appropriate cases documented in [21], [24] and [34]. The effect of the crack advance on the shape of the plastic zone is to constrict its width and to tilt the inclination of the zone towards the symmetry axis $(X_2 = 0)$. Between the nodal release steps and depending on the amount of load incrementation, the plastic zone attempts to restore the butterfly shape familiar from static crack analysis. The achievement of a steady state solution is particularly evident from results of the non-hardening case which includes two consecutive nodal release steps; there is negligible difference between the plastic zone shapes following these crack advance steps. The small, actively plastic wake region in the non-hardening case contrasts sharply with the lack of this region in the hardening cases. As has been remarked, this is attributed to the isotropic constitutive theory used in these analyses. Also, the angular tilt and plastic zone constriction are reminiscent of similar growth effects encountered in Mode III analyses, e.g., [9] and [17].

Material Strain Histories

The equivalent plastic strain history of a material point in the slip line fan above the crack tip before crack advance indicates a high amount of straining prior to crack advance, further straining during the first nodal release step and negligible further straining. The strain incurred during the first crack advance step is due to the fan region sweeping by the material point. A material point positionally similar with respect to the crack tip before the third crack advance step is not plastically strained until the crack has advanced sufficiently to engulf this point with its accompanying plastic zone. This element is then strained irreversibly, but less than the corresponding element in the stationary crack case. Ratios of

the plastic strain at the second material point prior to nodal release 3 divided by the plastic strain at the positionally similar material point prior to the first step of crack advance are 0.95, 0.92 and 0.87 for N = 0.0, 0.1 and 0.2 respectively. These values corroborate the observation of Rice [8] that the strain field associated with an extending crack sustains a weaker singularity than that associated with a stationary crack, r^{-1} versus $\ell n\ r^{-1}$ for the non-hardening case. The above ratios also imply that, at least for strain controlled ductile rupture mechanisms, the extent of stable crack growth is greater for a hardening material than for a non-hardening material.

Separation Energy Rates

Each of the nodal release steps provides a record of vertical displacement versus reaction force. Calculating the area under this curve and dividing by the finite crack advance step one obtains a separation energy rate, G^{Δ} in the notation of Kfouri and Rice [35]. It is the finite value of the crack advance step that renders this calculation non-trivial, for in the limit of growth step approaching zero and for materials which exhibit a finite stress level at the crack tip such a calculation yields zero for G^{Δ}, [36]. G^{Δ} values taken from the work of Kfouri and Miller [19] and McMeeking [3] together with values from the present analyses are plotted on figure 10. The points of Kfouri and Miller result from the plane strain analysis of the tensile and equibiaxial loading of a finite plate containing a crack. The ratio of crack length to plate width is 0.125 and the ratio of Young's modulus to initial yield stress is 667.7. Their analyses model the material as linear hardening with a tangent modulus equal to 0.023 times the elastic modulus and Poisson's ratio equal to 0.3. The points of

McMeeking are taken from separation energy rate calculations for the small scale yielding analysis of a blunted notch; material properties are $E/\sigma_o = 300$, Poisson's ratio = 0.3 and a power law hardening exponent N equal to 0.1. McMeeking's work includes finite strain effects at the blunted notch and employs crack growth steps on the order of the crack opening displacement, whereas the growth steps employed by Kfouri and Miller and the author are much larger. The "steady state" point of McMeeking corresponds to the final growth step calculated and it is presented for completeness although his analysis does not indicate that steady state conditions are achieved.

The explanation for the separate pattern of points due to Kfouri and Miller is thought to be the "T effect", which is explored by Larsson and Carlsson [34] and Rice [37]. The origin of the effect is the presence of non-vanishing, non-singular terms in the eigenvalue expansion of the elastic stress tensor at the crack tip in plane strain. The points corresponding to the equibiaxial tensile loading case of Kfouri and Miller provide the best fit with points from the present analyses. This is because the present formulation has $T = 0$ and for an infinite plate under equibiaxial loading, $T = 0$ (for a finite plate $T \approx 0$) . Kfouri and Rice [35] present a relation between J and G^{Δ} for the tensile load case in an effort to correlate the two quantities, but a subsequent communication with Kfouri has indicated a different relation for the equibiaxial loading case. The conclusion is that the use of J as a correlator of the separation energy during a finite growth step of the size they explored is sensitive to the non-zero, non-singular stress terms present at the crack tip in plane strain. Figure 10 also indicates that the value of G^{Δ} is sensitive to the degree of strain hardening. But, these observations are made for points corresponding to

growth step sizes far in excess of values comparable to the crack opening displacement. Since it is in a region of linear extent on the order of crack opening displacement that ductile fracture mechanisms such as void coalescence and localization of shear dominate, it would seem to be step sizes of this order that are of greatest interest. By using such small crack advance steps it may be investigated whether J correlates with G^{Δ} independently of T, the value of N and the extent of yielding; that is, do all the curves which are different for larger crack advance steps merge into a single curve for step sizes on the order of the crack openings displacement. At present, only the values reported by McMeeking have growth steps in this range. Of course, in such analyses finite strain considerations must be properly treated, McMeeking and Rice [38]. Due to the elastic unloading that occurs during crack advance, J should be correlated with G^{Δ} values for the initial nodal release; similar correlations with G^{Δ} values for subsequent nodal releases must be interpreted carefully due to the clouded meaning of J following crack extension.

Finally, a discussion of the validity of the G^{Δ} quantity is warranted. The nodal reaction force to be relaxed to zero is related to the stress field surrounding the crack tip. As this force is relaxed to zero, the appropriate nodal displacement is monitored so the work expended in the relaxation process may be calculated. The elastic unloading of the body and the accumulated strain at the crack tip influence this displacement. However, no size scale is inherent in this calculation except that imposed by the finite element mesh, and as such, the fundamental significance of G^{Δ} is obfuscated unless a direct correlation of the step of crack advance may be made to a microstructurally significant dimension such as the crack opening displacement. Although their model involves failure by cleavage, the

necessity of an appropriate size scale in a fracture criterion is emphasized by Ritchie et al. [39] who correlate the fracture toughness of mild steel with the achievement of a critical tensile stress over a distance on the order of the spacing of crack nucleating carbides.

CONCLUSIONS

The following conclusions are drawn from the present analyses:

(i) The advancing crack profiles are consistent with the theoretical result of a vertical tangent at the crack tip. Since this is a local effect, it may yet be possible to sensibly define a crack opening angle.

(ii) Extending cracks in hardening and non-hardening materials are subject to effectively the same stress distributions as geometrically similar stationary cracks. The strains accumulated ahead of a moving crack tip are less than those of a corresponding stationary crack in corroboration of the analytical work of Rice [7], [8].

(iii) The active plastic zone ahead of a growing crack constricts and tilts, paralleling the behavior predicted from analytic and numerical investigations of Mode III cracks.

(iv) For separation energy rates calculated for crack growth steps much greater than the nominal crack opening displacement, the use of J as a correlator is highly sensitive to strain hardening properties and the details of external loading.

(v) The incremental opening at the crack tip, due to load increase at fixed crack length, seems to be given by $d\delta = \alpha\, dJ/\sigma_o$; the value of α depends on material properties but is the same regardless of the extent of crack growth. Increments in crack surface displacement may be correlated with increments of crack growth at constant external load through the expression

$$d\delta = \frac{\sigma_o}{E}\, \beta\, \ell n \left[\frac{\lambda E J}{\sigma_o{}^2 r}\right] d\ell \quad .$$

The parameters β and λ are constant in these analyses.

Considerations which remain to be addressed are the effects of crack advance under increasing external load, the effects of different plasticity models on the present small scale yielding solutions and the effects of large scale, fully plastic specimen behavior. Also, the role of the finite strain at the root of a blunted crack should be further investigated in the extending crack situation.

ACKNOWLEDGEMENTS

This study was supported by the Energy Research and Development Agency under contract EY-76-S-02-3084 and by the NSF Materials Research Laboratory at Brown University. The author expresses his gratitude to Professor James R. Rice for his guidance in this study and his patience in reviewing this manuscript.

REFERENCES

[1] Rice, J.R., "Elastic-Plastic Fracture Mechanics," in The Mechanics of Fracture, F. Erdogan, Ed., American Society of Mechanical Engineers, AMD - Vol. 19, 1976, pp. 23-53.

[2] Rice, J.R. and Johnson, M.A., "The Role of Large Crack Tip Geometry Changes in Plane Strain Fracture," in Inelastic Behavior of Solids, M.F. Kanninen et al., Eds., McGraw-Hill, 1970, pp. 641-672.

[3] McMeeking, R.M., "Finite Deformation Analysis of Crack Tip Opening in Elastic-Plastic Materials and Implications for Fracture Initiation," Chapter 1 of Ph.D. Thesis, Brown University, also to appear in Journal of the Mechanics and Physics of Solids.

[4] Shih, C.F., "Small Scale Yielding Analysis of Mixed Mode Plane Strain Crack Problems," in Fracture Analysis, ASTM Special Technical Publication 560, 1974, pp. 187-210.

[5] McClintock, F.A., "Ductile Fracture Instability in Shear," Journal of Applied Mechanics, Vol. 25, 1958, pp. 582-588.

[6] McClintock, F.A. and Irwin, G.R., "Plasticity Aspects of Fracture Mechanics," in Fracture Toughness Testing and Its Applications, ASTM Special Technical Publication 381, 1965, pp. 84-113.

[7] Rice, J.R., "Mathematical Analysis in the Mechanics of Fracture," in Fracture: An Advanced Treatise, H. Liebowitz, Ed., Vol. 2, Academic Press, 1968, pp. 191-311.

[8] Rice, J.R., "Elastic Plastic Models for Stable Crack Growth," in Mechanics and Mechanisms of Crack Growth, (Proceedings of Conference at Cambridge, England, April 1973), M.J. May, Ed., British Steel Corporation Physical Metallurgy Centre Publication, 1975, pp. 14-39.

[9] Chitaley, A.D. and McClintock, F.A., "Elastic-Plastic Mechanics of Steady Crack Growth Under Anti-Plane Shear," Journal of the Mechanics and Physics of Solids, Vol. 19, 1971, pp. 147-163.

[10] Broek, D., "Some Considerations on Slow Crack Growth," International Journal of Fracture Mechanics, Vol. 4, 1968, pp. 19-29.

[11] Green, G., Smith, R.F. and Knott, J.F., "Metallurgical Factors in Low Temperature Slow Crack Growth," in Mechanics and Mechanisms of Crack Growth, (Proceedings of Conference at Cambridge, England, April 1973), M.J. May, Ed., British Steel Corporation Physical Metallurgy Centre Publication, 1975, pp. 40-54.

[12] Green, G. and Knott, J.F., "On Effects of Thickness on Ductile Crack Growth in Mild Steel," Journal of the Mechanics and Physics of Solids, Vol. 23, 1975, pp. 167-183.

[13] Clarke, G.A., Andrews, W.R., Paris, P.C. and Schmidt, D.W., "Single Specimen Tests for J_{IC} Determination," in Mechanics of Crack Growth, ASTM Special Technical Publication 590, 1976, pp. 27-42.

[14] Griffis, C.A. and Yoder, G.R., "Initial Crack Extension in Two Intermediate Strength Aluminum Alloys," Transactions ASME, Journal of Engineering Materials and Technology, Vol. 98, 1976, pp. 152-158.

[15] de Koning, A.U., "A Contribution to the Analysis of Slow Stable Crack Growth," presented at the 14th International Congress of Theoretical and Applied Mechanics, Delft, (also Report NLR MP 75035 U, National Aerospace Laboratory NLR, Amsterdam, The Netherlands), 1976.

[16] Andersson, H., "Finite Element Treatment of a Uniformly Moving Elastic-Plastic Crack Tip," Journal of the Mechanics and Physics of Solids, Vol. 22, 1974, pp. 285-308.

[17] Sorensen, E.P., "A Finite Element Investigation of Stable Crack Growth in Anti-Plane Strain," Brown University Report MRL E-106, August 1977. Also submitted for publication in the International Journal of Fracture.

[18] Andersson, H., "A Finite Element Representation of Stable Crack Growth," Journal of the Mechanics and Physics of Solids, Vol. 21, 1973, pp. 337-356.

[19] Kfouri, A.P. and Miller, K.J., "Crack Separation Energy Rates in Elastic-Plastic Fracture Mechanics," Proceedings of the Institution of Mechanical Engineers, Vol. 190, 1976, pp. 571-584.

[20] Hill, R., The Mathematical Theory of Plasticity, Oxford University Press, 1950.

[21] Tracey, D.M., "Finite Element Solutions for Crack Tip Behavior in Small Scale Yielding," Transactions ASME, Journal of Engineering Materials and Technology, Vol. 98, 1976, pp. 146-151.

[22] Rice, J.R. and Rosengren, G.F., "Plane Strain Deformation Near a Crack Tip in a Power Law Hardening Material," Journal of the Mechanics and Physics of Solids, Vol. 16, 1968, pp. 1-12.

[23] Marcal, P.V. and King, I.P., "Elastic-Plastic Analysis of Two Dimensional Stress Systems by the Finite Element Method," International Journal of Mechanical Sciences, Vol. 9, 1967, pp. 143-155.

[24] Rice, J.R. and Tracey, D.M., "Computational Fracture Mechanics," in Numerical and Computer Methods in Structural Mechanics, S.J. Fenves et al., Eds., Academic Press, 1973, pp. 585-623.

[25] Yang, W.H., "A Method for Updating the Cholesky Factorization of a Banded Matrix," Computer Methods in Applied Mechanics and Engineering, in press.

[26] Sorensen, E.P., "A Numerically Expedient Scheme for Elastic-Plastic Calculations in Incremental Finite Element Analysis," Computer Methods in Applied Mechanics and Engineering, in press.

[27] Sorensen, E.P., "Some Numerical Studies of Stable Crack Growth," Ph.D. Dissertation, Brown University.

[28] Turner, M.J., Clough, R.W., Martin, H.C. and Topp, L.J., "Stiffness and Deflection Analysis of Complex Structures," Journal of the Aeronautical Sciences, Vol. 9, 1956, pp. 805-823.

[29] Nagtegaal, J.C., Parks, D.M. and Rice, J.R., "On Numerically Accurate Finite Element Solutions in the Fully Plastic Range," Computer Methods in Applied Mechanics and Engineering, Vol. 4, 1974, pp. 153-177.

[30] Guyan, R.J., "Reduction of Stiffness and Mass Matrices," Journal of the American Institute of Aeronautics and Astronautics, Vol. 3, 1965, p. 380.

[31] Tracey, D.M., "Finite Elements for Determination of Crack Tip Elastic Stress Intensity Factors, " Engineering Fracture Mechanics, Vol. 3, 1971, pp. 255-265.

[32] Wilson, W.K., "Some Crack Tip Finite Elements for Plane Elasticity," in Stress Analysis and Growth of Cracks, ASTM Special Technical Publication 513, 1972, pp. 90-105.

[33] Parks, D.M., "Some Problems in Elastic-Plastic Finite Element Analysis of Cracks," Ph.D. Dissertation, Brown University, Chapter III.

[34] Larsson, S.G. and Carlsson, A.J., "Influence of Non-Singular Stress Terms and Specimen Geometry on Small Scale Yielding at Crack Tips in Elastic-Plastic Materials," Journal of the Mechanics and Physics of Solids, Vol. 21, 1973, pp. 263-277.

[35] Kfouri, A.P. and Rice, J.R., "Elastic Plastic Separation Energy Rates for Crack Advance in Finite Growth Steps," in Fracture 1977, D.M.R. Taplin et al., Eds., Solid Mechanics Division Publication, University of Waterloo, Vol. 1, 1977, pp. 43-59.

[36] Rice, J.R., "An Examination of the Fracture Mechanics Energy Balance from the Point of View of Continuum Mechanics," in Proceedings of 1st International Congress on Fracture, Sendai, Japan, T. Yokobori et al., Eds., Japanese Society for Strength and Fracture, Vol. 1, 1965, pp. 309-340.

[37] Rice, J.R., "Limitations to the Small Scale Yielding Approximation for Crack Tip Plasticity," Journal of the Mechanics and Physics of Solids, Vol. 22, 1974, pp. 17-26.

[38] McMeeking, R.M. and Rice, J.R., "Finite Element Formulations for Problems of Large Elastic-Plastic Deformation," International Journal of Solids and Structures, Vol. 11, 1965, pp. 601-616.

[39] Ritchie, R.O., Knott, J.F. and Rice, J.R., "On the Relationship Between Critical Tensile Stress and Fracture Toughness in Mild Steel," Journal of the Mechanics and Physics of Solids, Vol. 21, 1973, pp. 395-410.

sm

Table I : Crack Tip Opening Angles (radians)

	Release 1	Release 2	Release 3	Release 4	Release 5
N = 0.0	0.015	0.016	0.017	0.017	0.017
N = 0.1	0.016	0.017	0.018	0.018	-
N = 0.2	0.018	0.019	0.020	0.020	-

Table II : Values of α in the correlation of $d\delta$ and dJ/σ_o

		Measured Immediately Behind Current Tip			Measured at Original Tip Position		
	Initial Value	After Release 1	After Release 2	After Release 3	After Release 1	After Release 2	After Release 3
N = 0.0	0.66	0.65	0.66	0.66	0.65	0.60	0.60
N = 0.1	0.54	0.54	0.53	0.52	0.54	0.51	0.54
N = 0.2	0.44	0.43	0.43	0.41	0.43	0.41	0.46

LIST OF FIGURE CAPTIONS

Figure 1. Load histories applied to the present analyses.

Figure 2. Schematic representation of finite element grid and boundary conditions.

Figure 3. Arrangement of elements in fine mesh region.

Figure 4. Crack surface displacements, stationary and steady state advancing crack solutions for N=0.0, 0.1, and 0.2.

Figure 5. Evolution of crack surface displacements through the loading history of the non-hardening case.

Figure 6. Correlation between increments of crack opening displacement and J.

Figure 7. σ_{22} stress distributions ahead of the crack tip.

Figure 8. (A) Stress history of element C plotted versus crack advance for the non-hardening case.

(B) Prandtl slip line field stress distribution.

Figure 9. (A) Stationary and steady state plastic zone shapes for N = 0.0.

(B) Stationary and steady state plastic zone shaped for N = 0.1.

(C) Stationary and steady state plastic zone shapes for N = 0.2.

Figure 10. Separation energy rates correlated with J and plotted versus growth step.

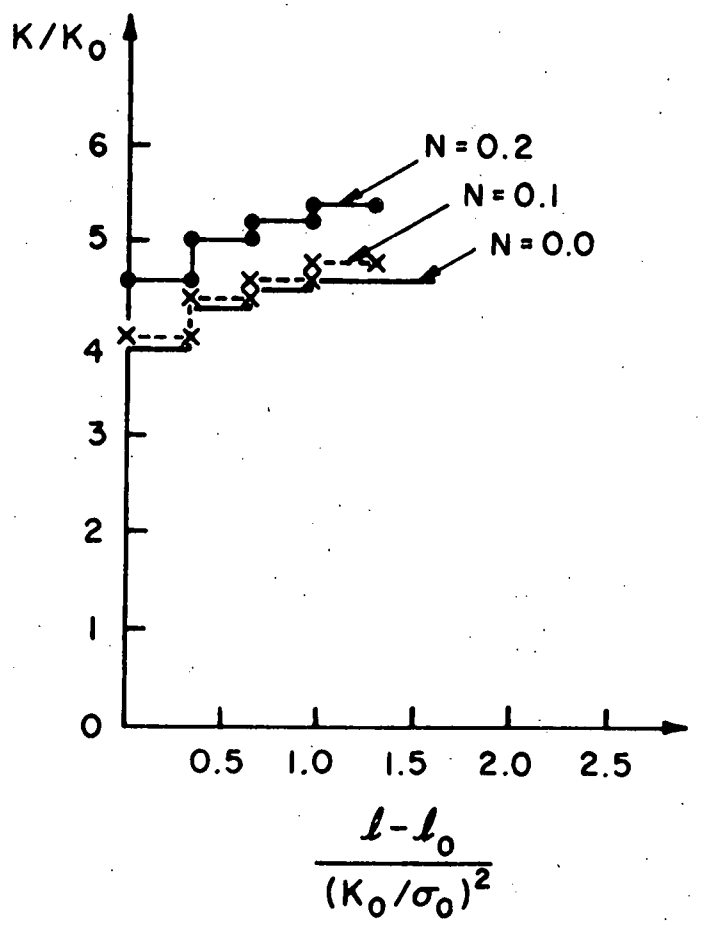

FIGURE 1

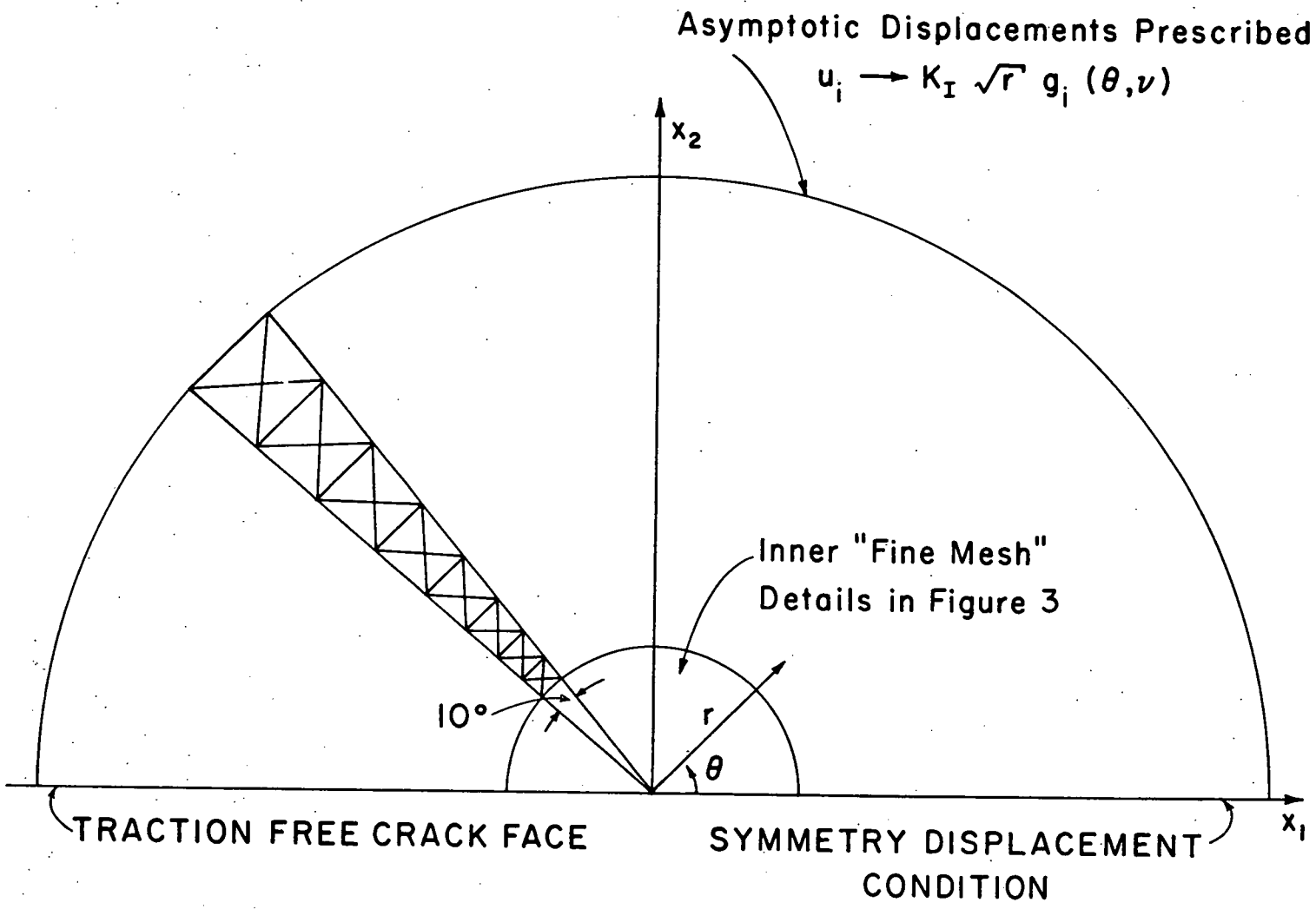
Asymptotic Displacements Prescribed
$u_i \rightarrow K_I \sqrt{r}\, g_i(\theta,\nu)$
x_2
Inner "Fine Mesh"
Details in Figure 3
10°
r
θ
TRACTION FREE CRACK FACE
SYMMETRY DISPLACEMENT CONDITION
x_1

FIGURE 2

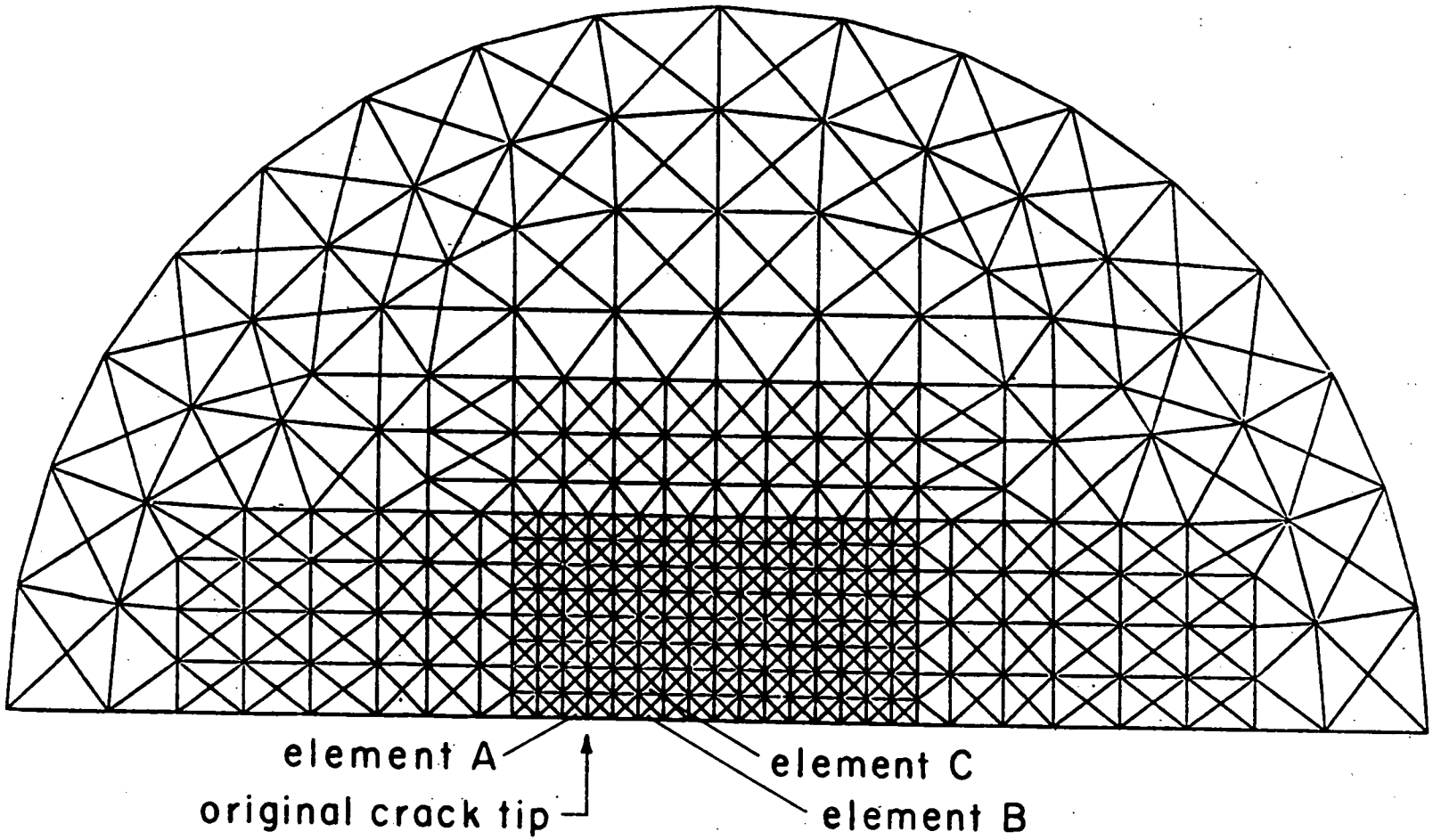

FIGURE 3

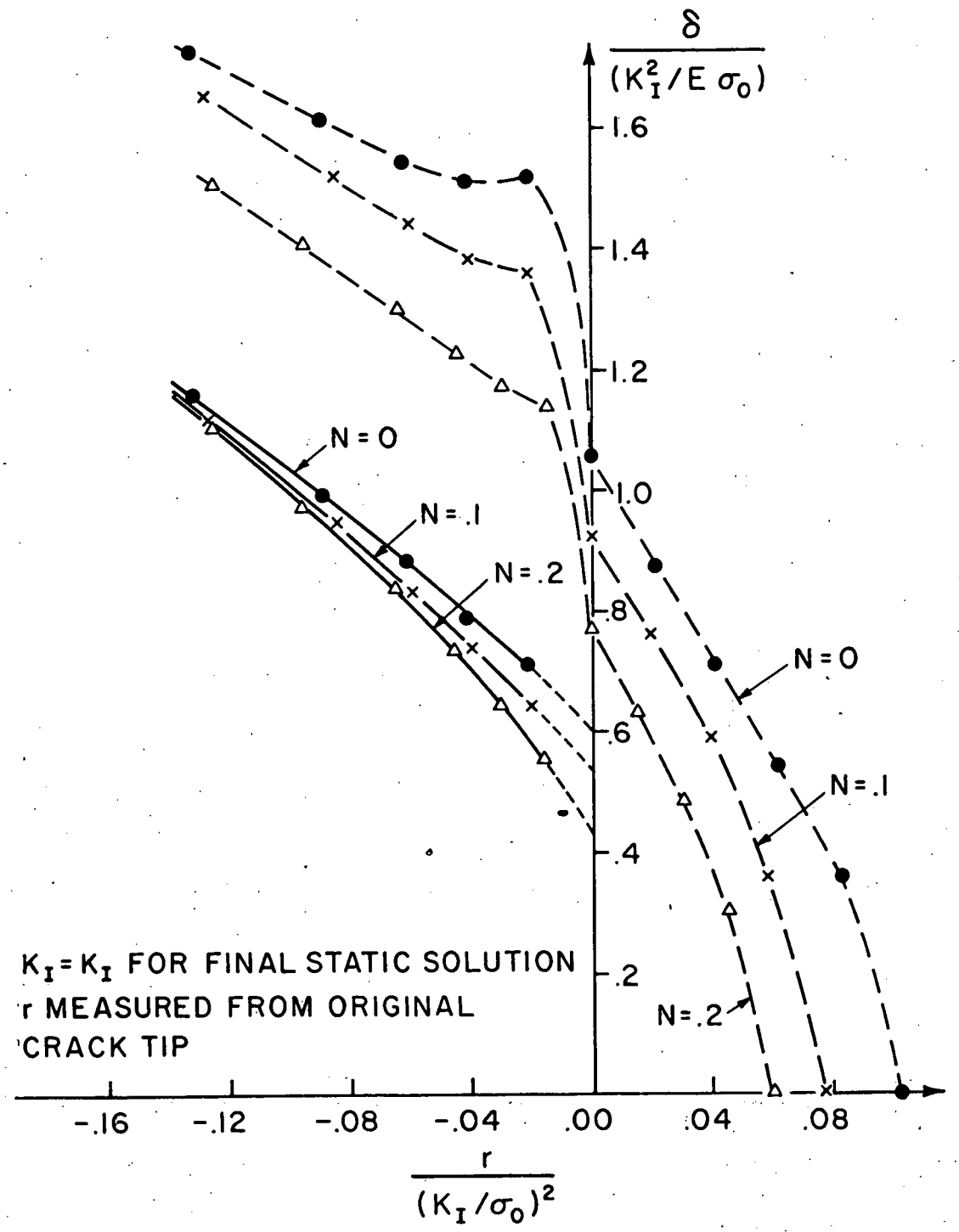
δ / (K_I^2 / E σ_0)
1.6
1.4
1.2
1.0
.8
.6
.4
.2
N = 0
N = .1
N = .2
N = 0
N = .1
N = .2
K_I = K_I FOR FINAL STATIC SOLUTION
r MEASURED FROM ORIGINAL CRACK TIP
-.16
-.12
-.08
-.04
.00
.04
.08
r / (K_I / σ_0)^2

FIGURE 4

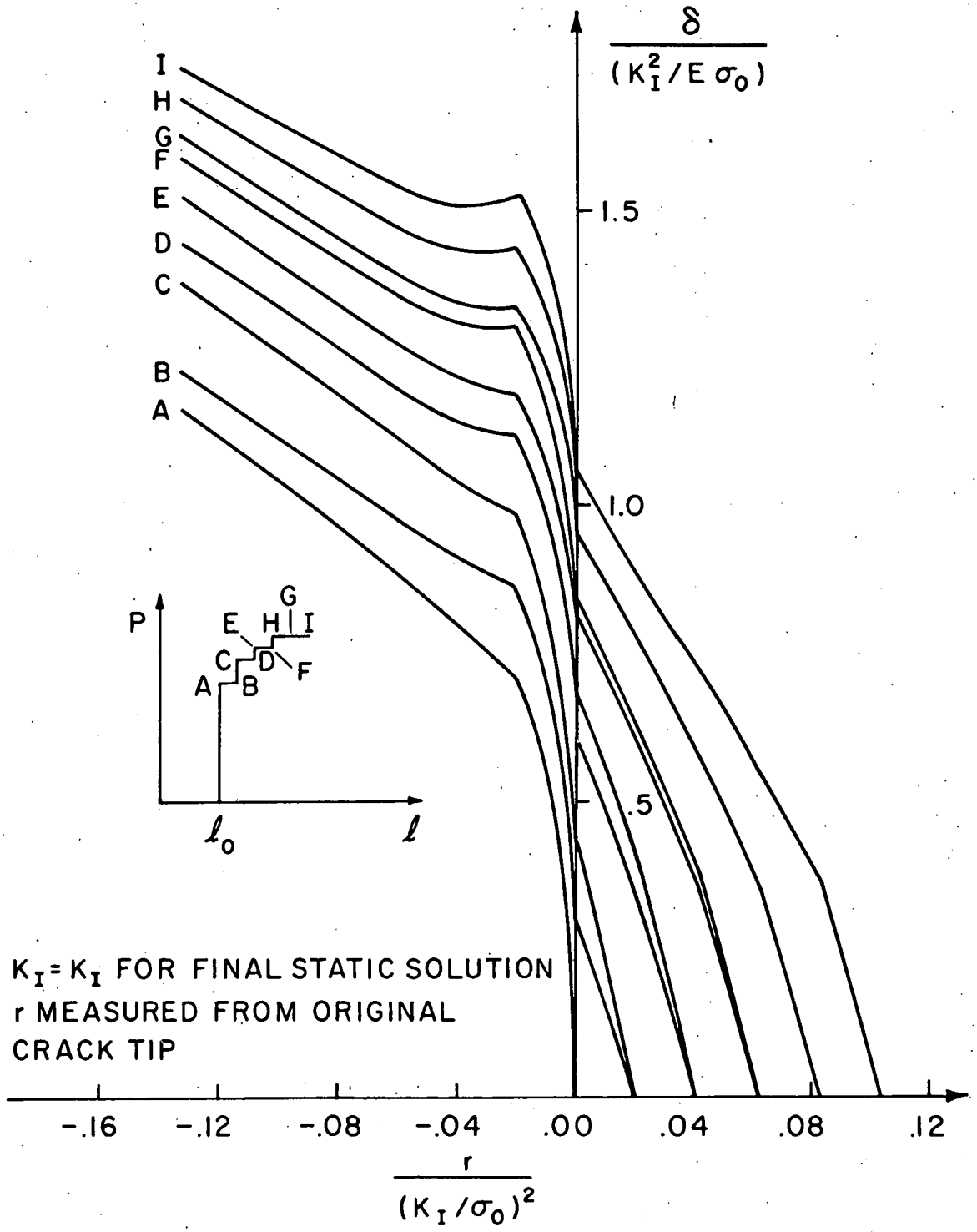
δ / (K_I^2 / E σ_0)
1.5
1.0
.5
I
H
G
F
E
D
C
B
A
P
G
E H I
C D F
A B
ℓ_0
ℓ
K_I = K_I FOR FINAL STATIC SOLUTION
r MEASURED FROM ORIGINAL CRACK TIP
-.16
-.12
-.08
-.04
.00
.04
.08
.12
r / (K_I / σ_0)^2

FIGURE 5

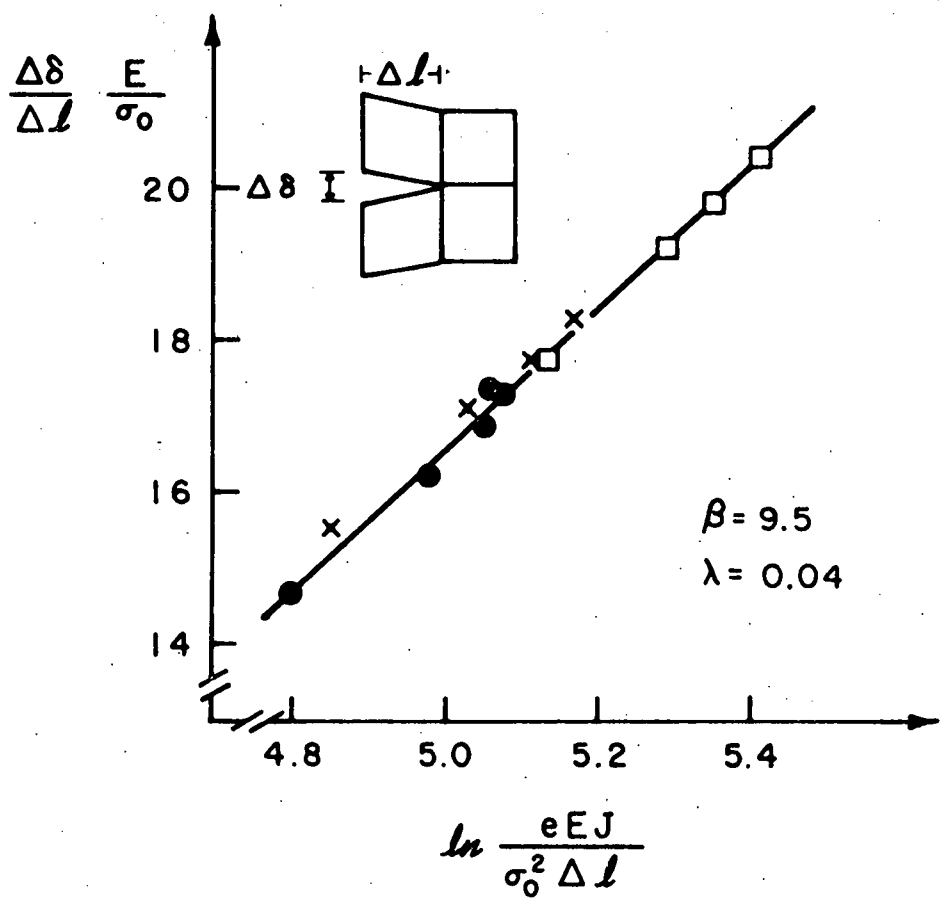
$\frac{\Delta\delta}{\Delta\ell}\ \frac{E}{\sigma_0}$
$\Delta\ell$
$\Delta\delta$
20
18
16
14
$\beta = 9.5$
$\lambda = 0.04$
4.8
5.0
5.2
5.4
$\ln \frac{eEJ}{\sigma_0^2 \Delta\ell}$

FIGURE 6

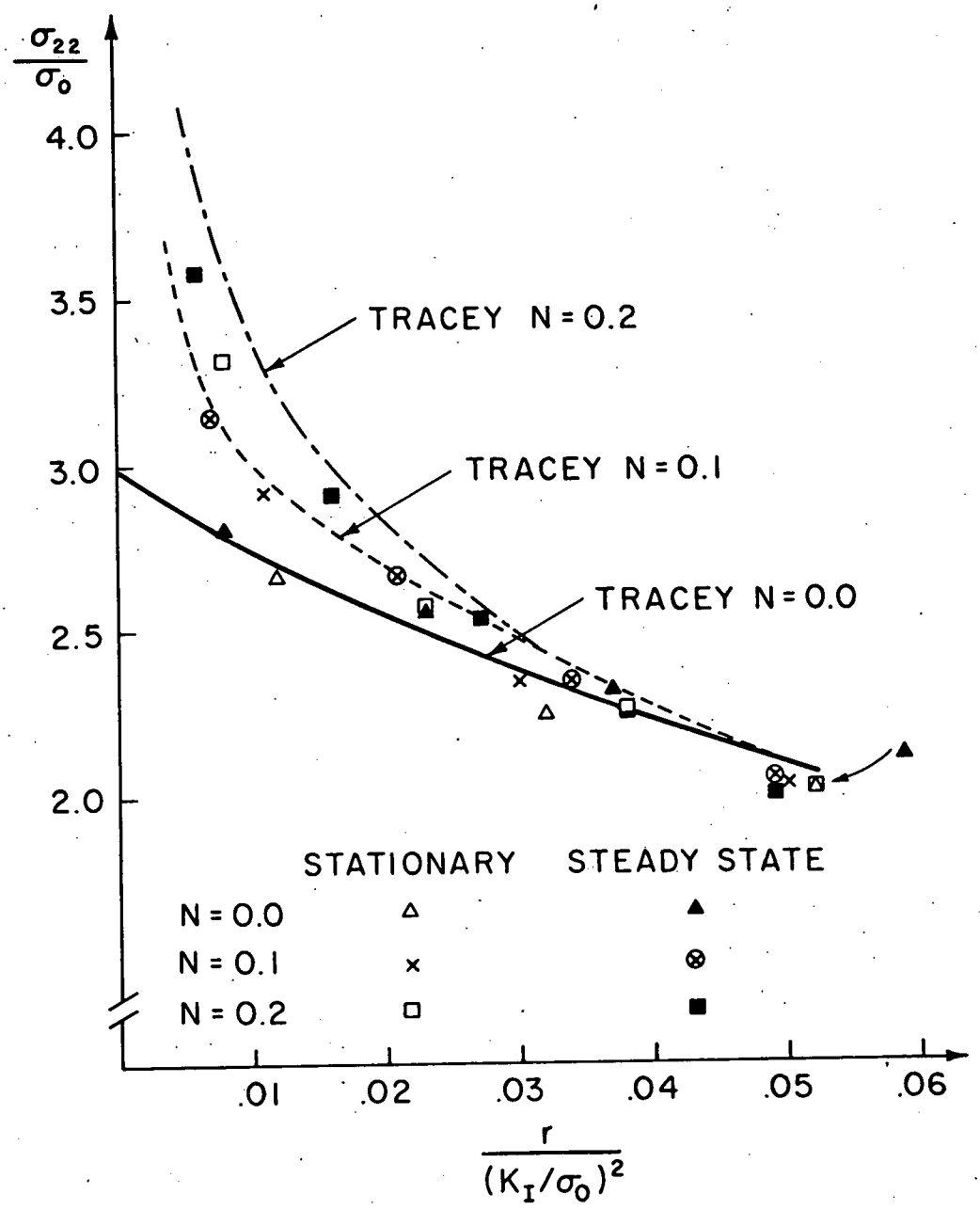
$\frac{\sigma_{22}}{\sigma_0}$
4.0
3.5
3.0
2.5
2.0
TRACEY N = 0.2
TRACEY N = 0.1
TRACEY N = 0.0
STATIONARY
STEADY STATE
N = 0.0
N = 0.1
N = 0.2
.01
.02
.03
.04
.05
.06
$\frac{r}{(K_I/\sigma_0)^2}$

FIGURE 7

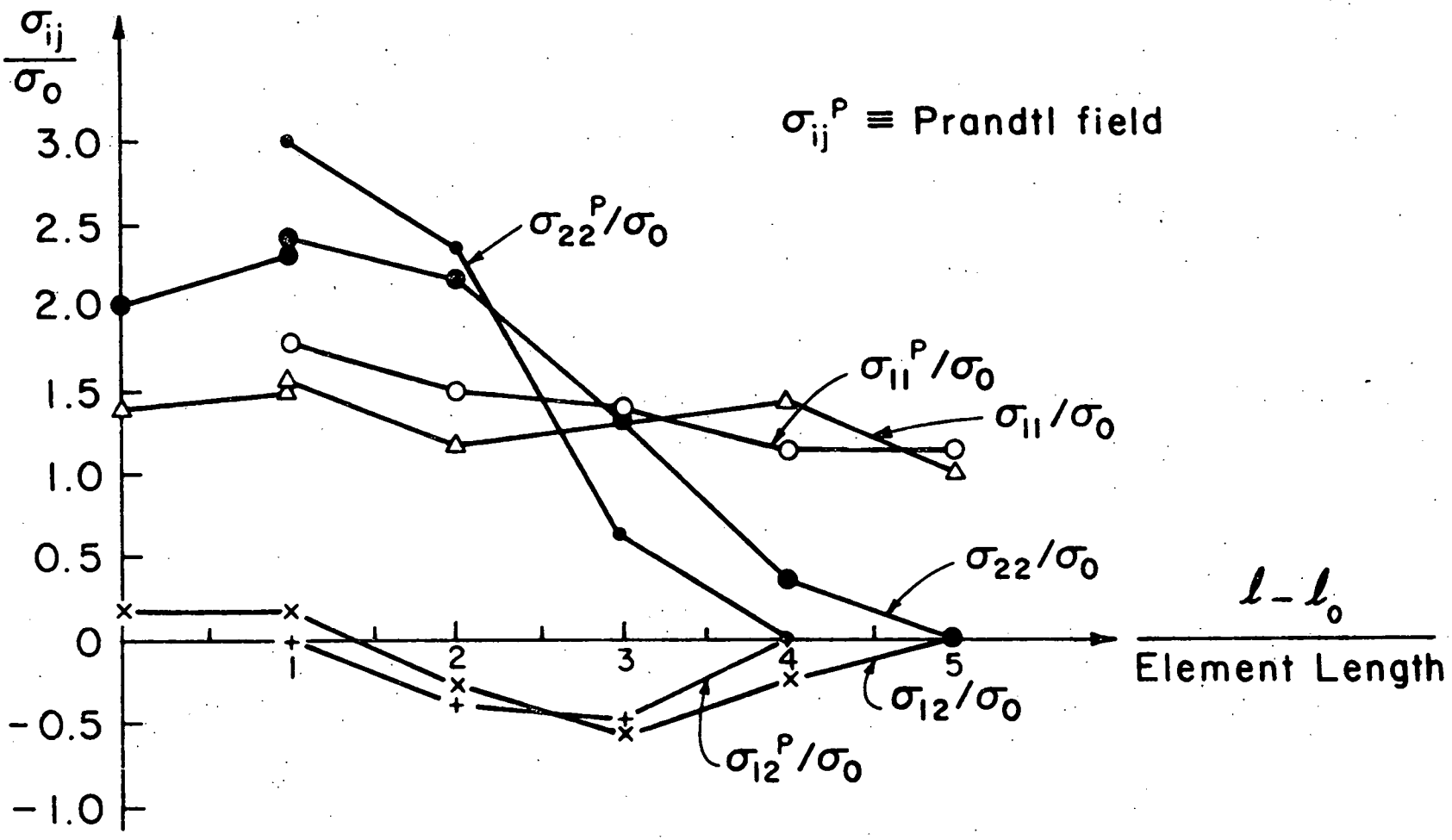
$\frac{\sigma_{ij}}{\sigma_0}$
3.0
2.5
2.0
1.5
1.0
0.5
0
-0.5
-1.0
1
2
3
4
5
$\sigma_{ij}^P \equiv$ Prandtl field
σ_{22}^P/σ_0
σ_{11}^P/σ_0
σ_{11}/σ_0
σ_{22}/σ_0
σ_{12}/σ_0
σ_{12}^P/σ_0
$\frac{l - l_0}{\text{Element Length}}$

FIGURE 8A

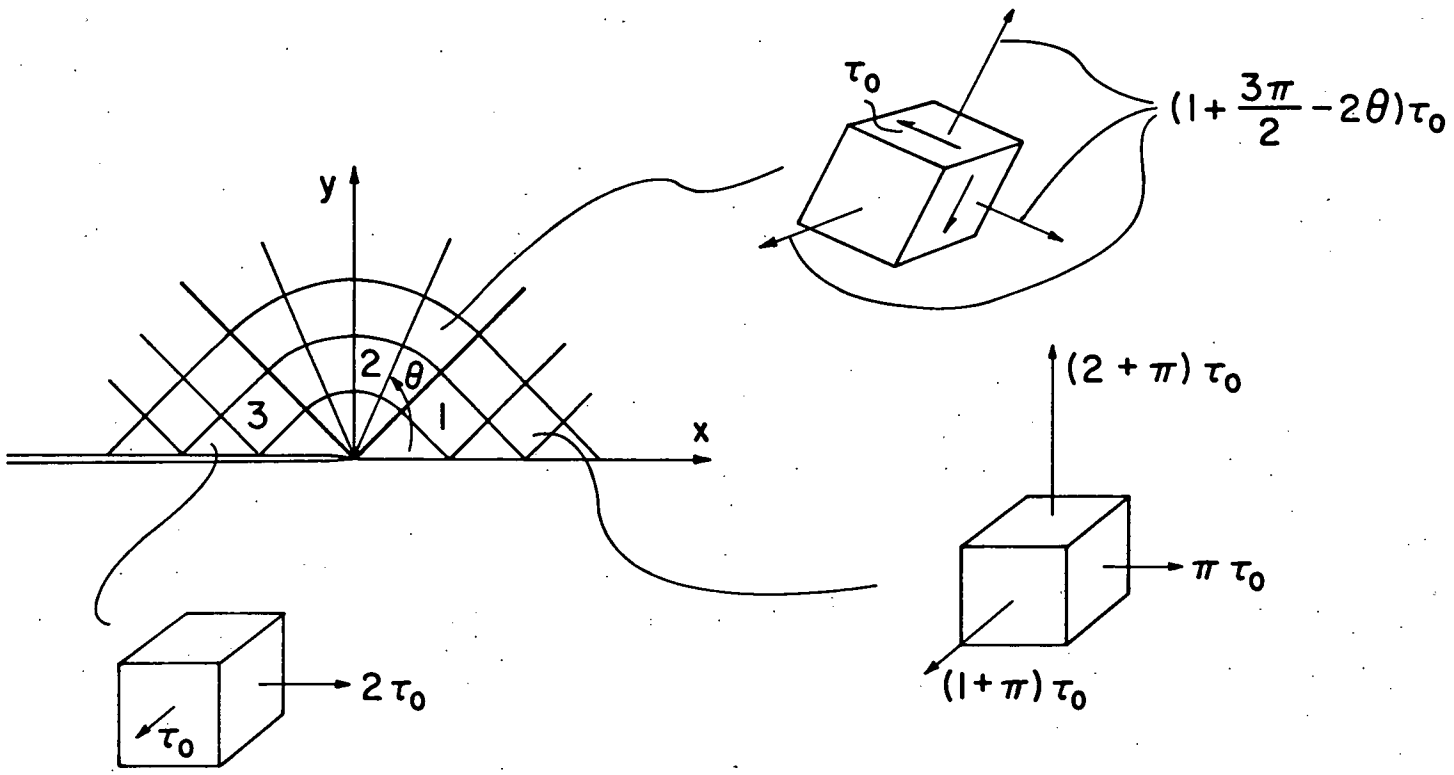
τ_0
$(1+\frac{3\pi}{2}-2\theta)\tau_0$
y
2
θ
3
1
x
$(2+\pi)\tau_0$
$\pi\tau_0$
$(1+\pi)\tau_0$
$2\tau_0$
τ_0

FIGURE 8B

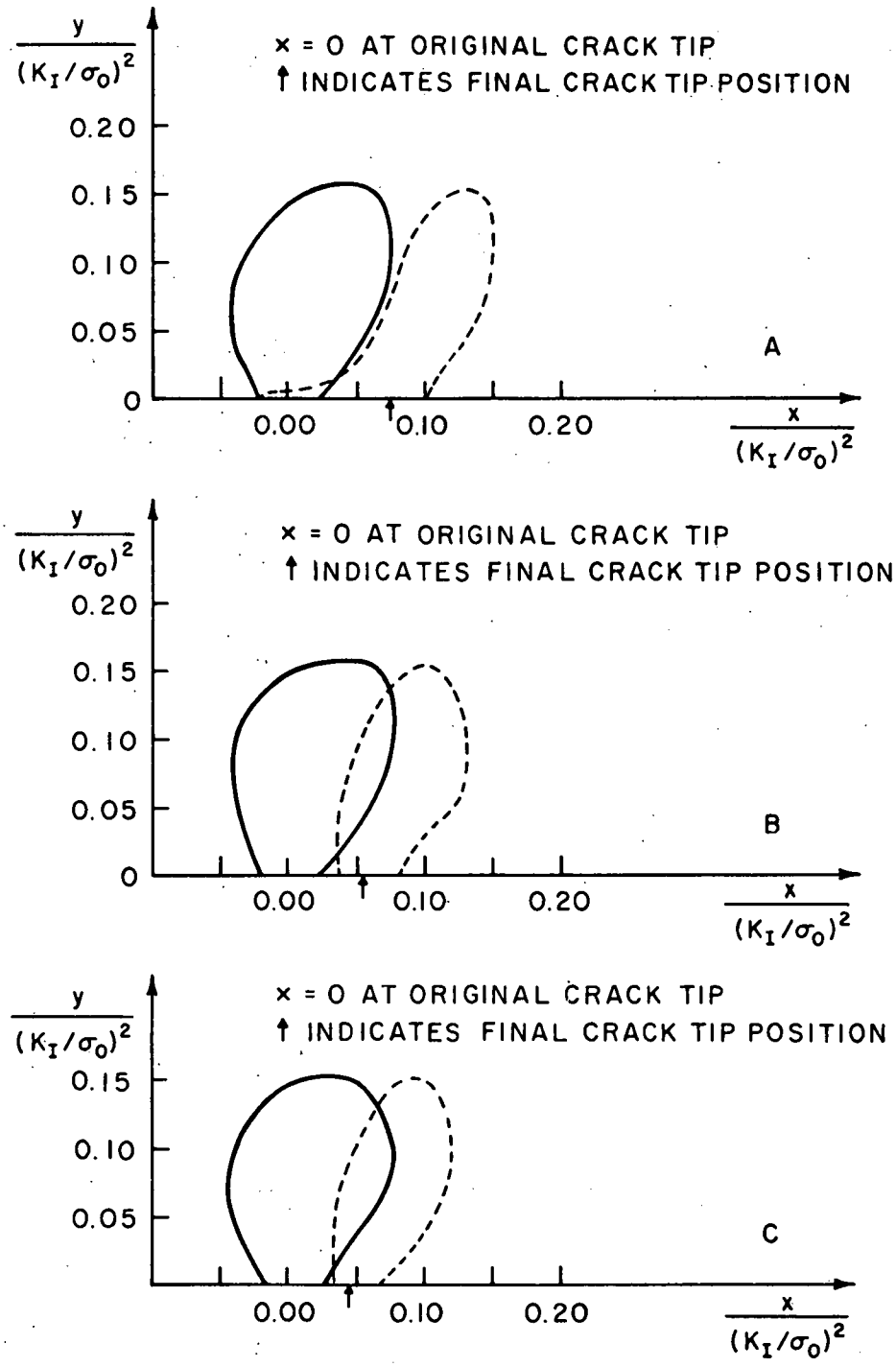
y / (K_I/σ_0)^2
x = 0 AT ORIGINAL CRACK TIP
↑ INDICATES FINAL CRACK TIP POSITION
0.20
0.15
0.10
0.05
0
0.00
0.10
0.20
x / (K_I/σ_0)^2
A
B
C

FIGURE 9

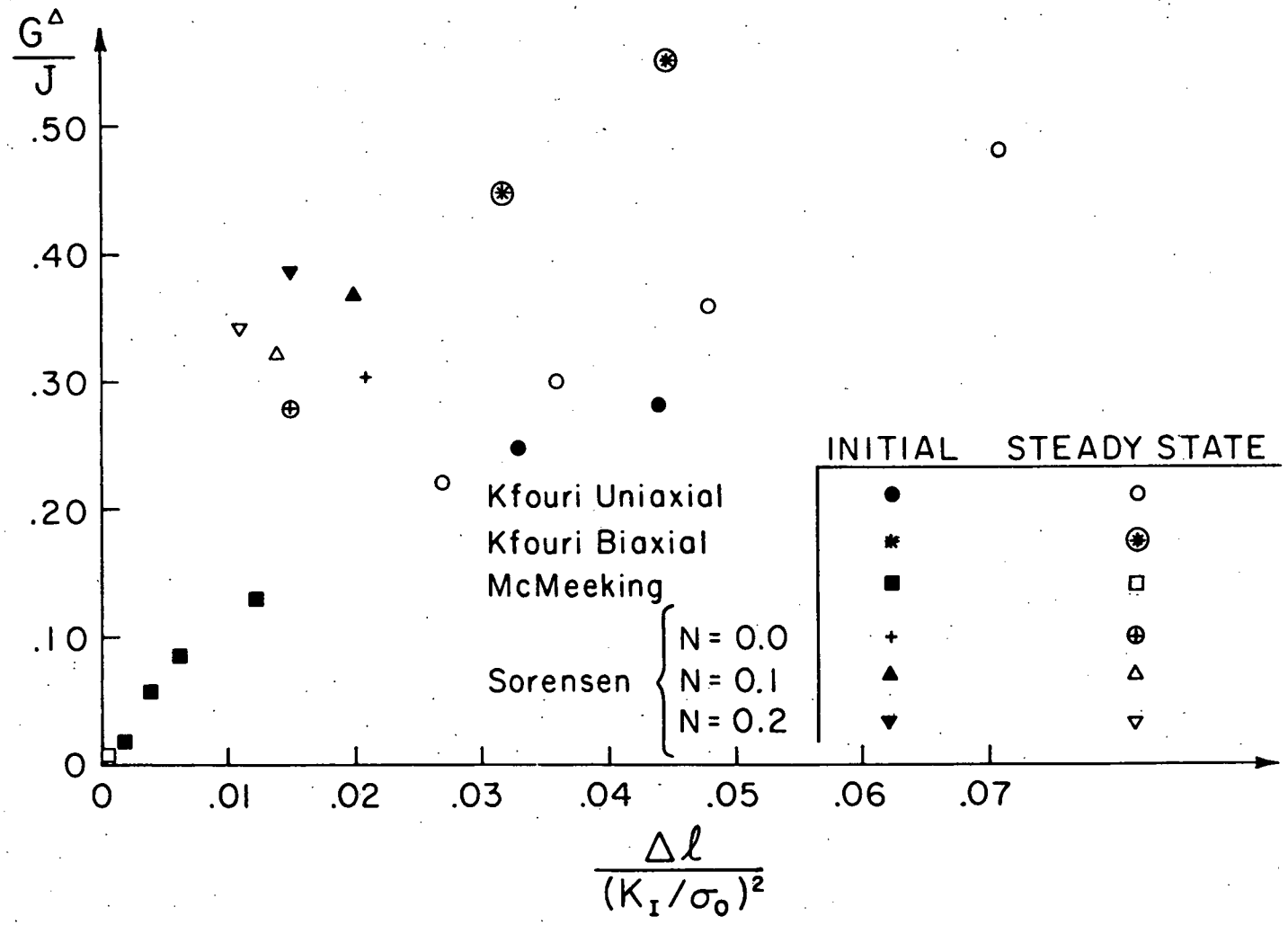
$\frac{G^{\Delta}}{J}$
.50
.40
.30
.20
.10
0
0
.01
.02
.03
.04
.05
.06
.07
$\frac{\Delta \ell}{(K_I/\sigma_0)^2}$
INITIAL
STEADY STATE
Kfouri Uniaxial
Kfouri Biaxial
McMeeking
Sorensen
N = 0.0
N = 0.1
N = 0.2

FIGURE 10